



LJMU Research Online

Jamal, M and Morgan, MN

Materials characterization part I: contact area of the Berkovich indenter for nanoindentation tests

<http://researchonline.ljmu.ac.uk/id/eprint/6134/>

Article

Citation (please note it is advisable to refer to the publisher's version if you intend to cite from this work)

Jamal, M and Morgan, MN (2017) Materials characterization part I: contact area of the Berkovich indenter for nanoindentation tests. International Journal of Advanced Manufacturing Technology. ISSN 0268-3768

LJMU has developed **LJMU Research Online** for users to access the research output of the University more effectively. Copyright © and Moral Rights for the papers on this site are retained by the individual authors and/or other copyright owners. Users may download and/or print one copy of any article(s) in LJMU Research Online to facilitate their private study or for non-commercial research. You may not engage in further distribution of the material or use it for any profit-making activities or any commercial gain.

The version presented here may differ from the published version or from the version of the record. Please see the repository URL above for details on accessing the published version and note that access may require a subscription.

For more information please contact researchonline@ljmu.ac.uk

<http://researchonline.ljmu.ac.uk/>

MATERIALS CHARACTERISATION PART I: CONTACT AREA OF THE BERKOVICH INDENTER FOR NANOINDENTATION TESTS

Jamal, M¹ and Morgan, M N²

¹ the manufacturing Technology Centre, Ansty, UK

² GERI, Liverpool John Moores University, Liverpool, UK

E-mail: mikdam.jamal@the-mtc.org ; m.n.morgan@ljmu.ac.uk

Abstract

This is the first of two papers associated with materials characterisation methods based on hardness testing. This paper presents a method to determine the area function of the Berkovich indenter used in nanoindentation hardness tests. The geometry and hence projected area of the indenter is known to affect the force-displacement response of a material during the loading and unloading stages. It is therefore important that the projected area is accurately defined to ensure determination of correct material hardness values. It is shown that values for the projected area determined from numerical methods applied to experimental data differ from values predicted inversely from theory based on the assumption of perfect tip geometry. This difference is attributed principally to a blunting of the tip, presenting as a tip radius. A simulation of the nanoindentation hardness test system is developed using finite element modelling (FEM) methods. Solutions for a range of load indentation curves obtained from experiment with fused silica are determined from best fit analyses using the root mean square error objective function (RMSE). A linear regression method is subsequently developed and used to estimate the area function. A parametric study of simulation and experimental results has been completed to verify the FEM and to assess the influence of varying tip curvature on force-displacement response during the loading and unloading stages and is summarily reported. A new method of analysis for determination of area function is proposed for use with numerical based simulations, which for the first time, accommodates variation in tip geometry and which is shown to deliver improved agreement with nanoindentation experimental results. The second paper will focus on the study of the tip geometry of the Vickers micro-indenter.

Keywords: Berkovich indenter; Nanoindentation; finite element modelling (FEM); Elastic-plastic; fused silica

1 INTRODUCTION

Nanoindentation techniques are widely used to investigate the mechanical behaviour of a broad range of materials at the nanoscale. The load–displacement relationship is obtained from a plot of recorded information on forces and depth. The results of such tests [1 – 4] among many others are used to determine the elastic-plastic material properties: yield stress (σ_y), Young's Modulus (E), work hardening exponent (n) and hardness H . Several methods have been developed to analyse the loading-unloading curves of nanoindentation tests, the most important being those of [2, 3]. According to Oliver and Pharr, the reduced modulus Er , and the hardness are obtained

$$H = \frac{P_{max}}{A} \quad (1)$$

$$S_s = \frac{2\delta}{\sqrt{\pi}} Er \sqrt{A} \quad (2)$$

$$E = \frac{1-\nu^2}{E} + \frac{1-\nu_i^2}{E_i} \quad (3)$$

where P_{max} is the maximum indentation load, A is the projected contact area, S_s is stiffness at maximum indentation depth, and δ is a correction factor of the indenter uniaxial symmetry [5]. E and ν are the Young's Modulus and Poisson ratio for the test material, E_i and ν_i are the Young's Modulus and Poisson's ratio for the indenter.

Due to inconsistency in manufacture and because of wear through use in measurements, the indenter tip will invariably possess a finite radius of curvature. When the indentation depth is small, most, if not all, of the contact occurs in the highest spherical depth range, and the real contact area is different from that assumed for the indenter. In the case of nanoindentation tests, where penetration depth is comparatively small, this difference has a greater effect on accuracy. Therefore, in such a case, the area function needs to be calibrated for a range of indentation depths. Moreover, in the FEM simulation of nanoindentation and microindentation processes, the corresponding indenter tip radius needs to be fully specified in order to obtain a precise and simple geometrical shape of indenter.

Experimental investigations conducted over many years on many material systems have shown that the projected area A is an important parameter for obtaining mechanical properties. The projected area is considered to be a function of contact depth, $f(h_c)$ - obtained by calculating the shape of the indenter at intervals of contact depth. A calibration method has been proposed to estimate $f(h_c)$ prior to analysis of the projected area [3]. The estimation employs a pre-defined material of a known Young's Modulus and also takes into account compliance of the load structure. The area function is then estimated from the best fit for the A versus h_c data using the relationship:

$$A(h_c) = C_0 h_c^2 + C_1 h_c^1 + C_2 h_c^{1/2} + C_3 h_c^{1/4} + C_4 h_c^{1/8} + C_5 h_c^{1/16} \quad (4)$$

-where h_c is the contact depth, C_0 is the tip geometry coefficient ($C_0 = 24.5$ for a perfect Berkovich indenter, $C_1 - C_5$ are variable coefficients obtained from the indentation instrument at the calibration stage through a best fit of the experimental data. The Oliver and Pharr method is reported to be highly accurate in determining the area function of both simple and complex imprint shapes, however, in the actual application it is very difficult to understand the physical meaning of the coefficients introduced in Eq. (4).

Oliver and Pharr 1992 focussed on the calibration process to determine the area function; other researchers have suggested imaging techniques of the residual imprint for obtaining the tip geometry. Transmission electron microscopy (TEM) was employed by [2] who adapted a method developed earlier by [6] using two-stage carbon replicas to determine the indenter shape calibration. McElhaney [7] advocated a new indenter tip geometry calibration technique based on measurement of the compliance of both contacts and use of scanning electron microscopy (SEM) measurements for the areas of large indentations. Hermann [8] proposed a method to determine the indenter area function from direct measurements obtained using a scanning force microscope (SFM). The SFM data for tungsten and fused silica reference materials were reported to exhibit good agreement with results obtained from the compliance method of Oliver and Pharr.

The mathematical analysis of the load-displacement curve such as that described by Oliver and Pharr is relatively difficult for a complex material model and hence the strength of the interactions of the system are difficult to discern. However finite element modelling simulations are now more commonly employed to aid in the analysis of mechanical properties over a wide range of material systems using load-displacement curves obtained from experiment.

In this study, the area function was determined from continuous stiffness measurement (CSM) Berkovich nanoindentation tests with fused silica. It was reasonably assumed that the test material possessed a load-independent hardness. A FEM simulation was developed in order to aid determination of tip radius curvature and inclination angle distortion. The area function was analysed using experimental data coupled with FEM, and the deviation from the perfect Berkovich geometry was determined. The deviation being attributed to indenter tip blunting and inclination angle distortion. The developed FEM was subsequently adapted with a root mean square optimization algorithm in order to obtain the most accurate values of tip geometry for a range of target curvatures and apex angle. The method results in a best match (curve fitting) of both numerical and experimental results for a minimum value of objective function. This new approach, summarised in the flowchart of Figure 1, will be shown to improve the correlation between measurement and theory.

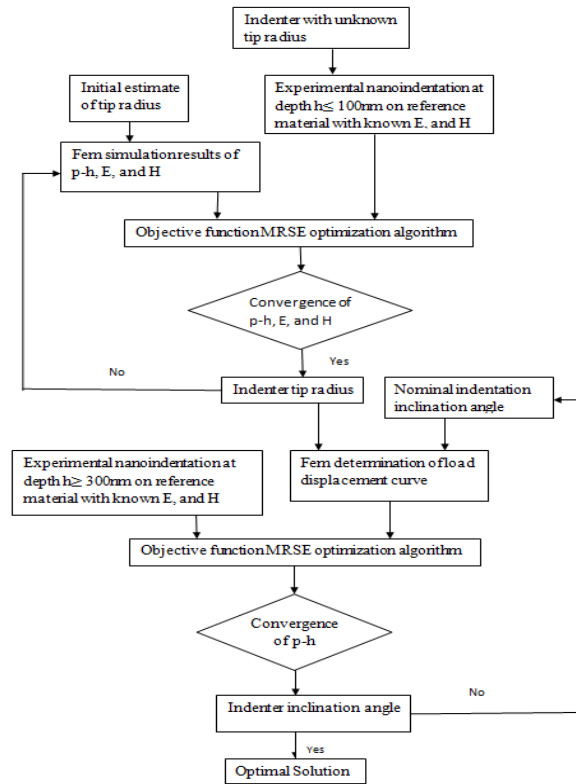


Figure 1 Flowchart of the global approach to determination of Berkovich indenter tip geometry and inclination angle

The flowchart in Figure 1 shows the global approach to determination of Berkovich indenter tip geometry and inclination angle. The approach associates experimental results, numerical results and an optimization algorithm with the FEM in order to obtain the optimal value for a wide range of simulation space and target parameters leading to a best match between experiment and theory (minimum objective function). Within this approach a parametric study was undertaken to determine the tip radius and inclination angle for a given set of indentation data using script programming language (python) interfaced with ABAQUS FEM. In this arrangement, the programme automatically searches for a range of values of tip radius and inclination angle until minimum convergence of load displacement is achieved. In the searching process, the input data was transformed to a discrete form with equally spaced points at each indentation depth (indentation points). At each indentation point the objective function values are calculated for each set of tip radius and inclination angle using a predefined program in Microsoft Excel. The final objective function was determined by the sum of objective functions at each indentation point. The final tip geometry is given by the minimum objective function value, defined as the optimal solution.

2 NANOINDENTATION TESTS: EXPERIMENTAL PROCEDURE

A fused silica sample was employed as the test specimen. The specimen was prepared to standard metallographic and nanoindentation test specification. The specimens were mounted using a hot compression thermosetting resin, machine type: Struers Prontopress-2. The specimen was positioned in the press mount, and the resin was added to a pre-defined level. Heat and pressure were then applied to set the specimen. The mounted specimen was finish prepared by wet grinding using a Metaserv rotary grinding machine with abrasive papers of grade P120 to fine grade P1200A. Nanoindentation experiments were carried out using a calibrated Nanoindenter CSM equipped with a standard Berkovich indenter. For each loading unloading cycle, an approach speed of 3000 nm/min and dwell time of 3 seconds at each load interval was programmed. Tests were carried out at ten pre-determined maximum load values in the range 6.5-250 mN. Three indentation tests were performed at each load, the average of the group results are presented in this study with thermal drift neglected. Typical load indentation curves obtained from this experimental work are shown in Figure 2 and Figure 3.

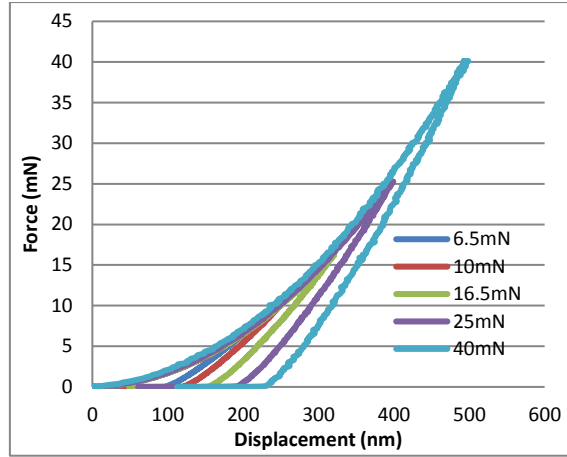


Figure 2 Typical loading- unloading curves for fused silica

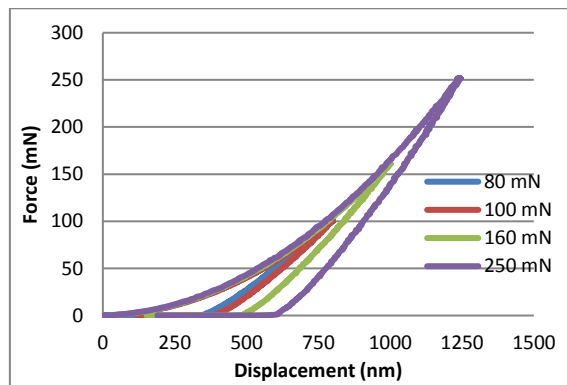


Figure 3 Typical loading- unloading curves for fused silica

3 NANOINDENTATION TESTS: RESULTS AND DISCUSSION

Fused silica was selected as the reference material because it has elastic isentropic properties and presents no significant plow profile (pile-up), for an indentation ratio of $\frac{h_f}{h_{max}} < 0.7$ - such properties can be expected to give an accurate projected area result from the Oliver and Pharr method. Beyond this value the correlation deteriorates [9, 10].

The method to determine the area function is based on the assumption of (a) load independent hardness for an elastic plastic material and (b) an elastic modulus independent of indentation depth.

Substitute Eq. (1) in Eq. (2) to give

$$S_s = \frac{2\delta}{\sqrt{\pi}} E_r \sqrt{\frac{P_{max}}{H}} \quad (5)$$

Based on the assumptions of (a) and (b) above

$$\beta = \frac{\sqrt{\pi} \sqrt{H}}{2\delta E_r} \quad (6)$$

The Oliver and Pharr method proposes the load frame and specimens as two springs in series

$$C_T = C_S + C_F \quad (7)$$

where C_T is the total compliance and is the sum of compliance of the specimen C_S and compliance of the frame structure, C_F . Based on the guiding principle given in Annex B of ISO14577-2 [11] it is possible to calculate the

indenter area function following the series of equations expressed therein. The specimen compliance during the elastic contact is specified by the inverse of the contact stiffness, and the total compliance is determined by the inverse of the initial region of the experimental unloading slope

$$\frac{1}{S_T} = \frac{1}{S_S} + C_F \quad (8)$$

Substitute Eq. (5), and Eq. (6) into Eq. (8) gives

$$\frac{1}{S_T} = \beta \frac{1}{\sqrt{P_{max}}} + C_F \quad (9)$$

To calculate the contact stiffness at maximum load S_T , Oliver and Pharr suggested that the first portion of the experimental unloading curve can be fitted to a power law mathematical expression

$$P = \alpha (h - h_f)^m \quad (10)$$

-where h is the indentation depth, h_f is the final indentation depth obtained by curve fitting, α and m are constants and can be determined using a least squares fit. The initial experimental unloading slope will be then obtained by differentiating Eq. (10) at maximum indentation depth

$$S_T = \left(\frac{dp}{dh} \right)_{h_{max}} = m\alpha (h - h_f)^{m-1} \quad (11)$$

Different indentation loads were applied to the fused silica specimens and the load displacement curves were analysed using Eq. (10) and Eq. (11) to determine the slope of the initial unloading curve S_T . Figure 4 shows the relation between the initial loading curve S_T and maximum applied load, P_{max} . As displayed, there exists a very good linear relationship between the inverse of the slope of the initial unloading curve, $1/S_T$ and the inverse of the square root of maximum load $(1/P_{max})^{0.5}$. The linear regression fitted data obtained from Eq. (8) gives $C_F = 0.128$ nm/mN, and $\beta = 32.05$ nm/mN. The load frame compliance shows a reasonable value for an instrumented nanoindentation measurement when compared with published data, for example: $C_F = 0.196$ nm/mN [12], and $C_F = 0.1$ nm/mN, [13].

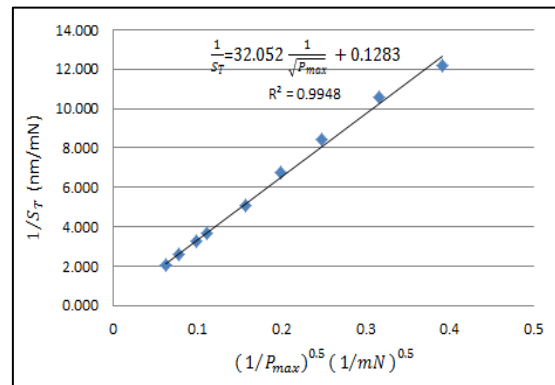


Figure 4 Relation between $1 / S_T$ and $(1/P_{max})^{0.5}$

4 THEORETICAL DEVELOPMENT

4.1 Berkovich Indenter Correction Factor

The value of the correction factor δ has a great effect on the elastic modulus, hardness and contact area function. For a small deformation of an elastic-plastic material caused by an indenter of a rigid asymmetric smooth profile, the value of δ is approximately unity, however for a Berkovich indenter with non-symmetric profile, the value of δ should be carefully considered in order to achieve a high accuracy in properties of hardness and Young's modulus. The latest studies have shown that for an elastic-plastic material and a perfectly elastic deformation by a rigid cone all estimated values of δ deviate from unity due to departures from the small strain

approximation. King [14] used a numerical method to study the effect of flat ended punches on the elastic material. The analysis showed that δ has a value of approximately 1.034 for a triangular punch and approximately 1.012 for a square based indenter. Vlassak and Nix [15] proposed a new numerical method using a triangular punch; and found a higher value of δ equal to 1.058. Hay [16] employed both an analytical technique and FEM to examine the deformation of elastic material by a conical indenter with a half induced angle of 70.3° , results show that in the case of Poisson's ratio of 0.3, δ deviates from unity by 0.067. They developed the following expression to calculate δ based on the conical indenter, induced angle size and Poisson's ratio

$$\delta = \pi \frac{[\frac{\pi}{2} - 0.8312 \cot \theta \frac{1-2\nu}{4(1-2\nu)}]}{[\frac{\pi}{2} - 0.8312 \cot \theta \frac{1-2\nu}{4(1-2\nu)}]^2} \quad (12)$$

From the review of previous works and removing the value derived from a flat half space, values for δ lie in the range $1.022 < \delta < 1.083$. However the value of $\delta = 1.05$ is considered a best target for this study given the possible error has a minimum value of approximately ± 0.05 .

4.2 Contact Area of a Berkovich Indenter

Determining the tip area function is essential to calculate the hardness and Young's modulus of the indented material, [3, 8]. There are different methods described in ISO 14577-4 that explain the procedure for tip area function calibration based on the mechanical properties of the indented material and prior understanding of the frame compliance.

The Young's Modulus and Poisson's ratio for fused silica are: $E = 70.2$ GPa and $\nu = 0.22$ respectively, [17]. The properties of the Berkovich indenter used in the experiment were Young's Modulus, $E_i = 1147$ GPa and Poisson's ratio $\nu_i = 0.07$ (as shown in the CSM data sheet). Based on this information the reduced modulus E_r from Eq. (3) was calculated to be 69.15 GPa. The hardness of the fused silica material employed in experiments was found from Eq. (6) to be $H = 6.96$ GPa and $\beta = 32.057$ nm/mN. Using this hardness value and value of β , the projected area can then be calculated using Eq. (1). It is first necessary to determine the contact depth h_c at each load for the relationship between h_c and P_{max} .

The contact depth h_c is given by the expression.

$$h_c = h_{max} - \varepsilon \frac{P_{max}}{S_s} \quad (13)$$

-where ε is a constant depending on indenter geometry. The contact depth was calculated based on the Oliver Pharr least square fitting procedure taking into account the correction factor. The exponent m , appearing in the Oliver Pharr method was calculated from curve fitting the first portion of the unloading curve and it has a great effect on the value of ε as indicated from Eq. (14).

$$\varepsilon = m \left[1 - \frac{2\Delta \left(\frac{m}{2(m-1)} \right)}{\sqrt{\pi} \Delta \left(\frac{m}{2(m-1)} \right)} (m-1) \right] \quad (14)$$

Over the expected range of $1.2 < m < 1.6$, the value of ε has been found to change in magnitude. The two values: $\varepsilon = 0.75$ proposed by Oliver Pharr and $\varepsilon = 0.785$ proposed by [13, 18] were reported as the maximum limits for ε variation.

Figure 5 shows the relationship between the unloading curve exponent m , and the maximum indentation depth with a fused silica specimen. A systematic relationship was observed where the exponent m , increased with a decrease in maximum indentation depth for an elastic-perfectly plastic material and the trend line remains relatively constant at maximum depths greater than 1000nm. These results agree with results obtained by [3, 9].

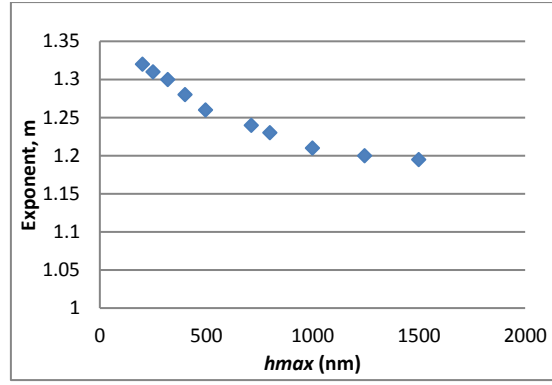


Figure 5 Relationship between the unloading curve exponent, m , and the maximum indentation depth for fused silica material

The hardness number obtained from Eq. (1) was used to calculate the projected contact area A as a function of the contact depth h_c , Eq. (13) and the results are shown in Figure 6. A linear relationship between \sqrt{A} and h_c for the actual and a perfect indenter is evident from the regression analysis.

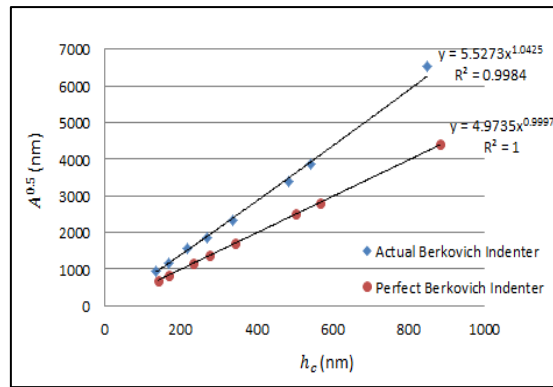


Figure 6 Tip area function values for a Berkovich tip determined from experiment compared to those for a perfect indenter

The Berkovich indenter is usually modelled as a rigid body with a perfect pyramidal shape having a half induced angle φ of 70.3° , the projected contact area / depth relationship proposed by [2] is:

$$A_p = \pi h_c^2 \tan^2 \varphi = 24.5 h_c^2 \quad (15)$$

As demonstrated in Figure 7, the actual indenter is in practice never an ideal indenter due to tip blunting. In the case of a non-perfect indenter, the indenter area functions as described by [18] and [19], can be determined from

$$A_p = C (h_c + h_d)^2 \quad (16)$$

Where h_d is the distance between the blunted edge and the cone-end as is shown in Figure 6. This distance is affected by the modification of indenter inclination angle. The expression for A_p in Eq. (16) is the projected area for a conical shape satisfying $h_c > \partial$. Regression analysis data shown in Figure 6 were obtained according to Eq. (16) using Sigma plot software, yielding values of $C = 30.55$ and $h_d = 12.5$.

The projected area of the spherical part A_{PS} of the indenter was calculated using Pythagorean theory for the case of $h_c \leq \partial$

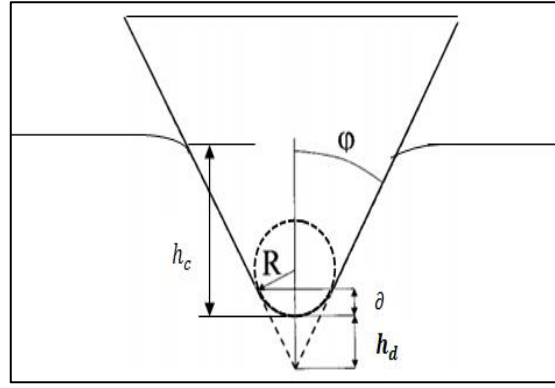


Figure 7 Schematic diagram shows the geometry of blunt indenter

The radius r of the spherical area is given by

$$A_{PS} = \pi r^2 \quad (17)$$

$$r^2 = R^2 - (R - h_c)^2 \quad (18)$$

$$h_d = \frac{R}{\sin\phi} - R \quad (19)$$

Substituting Eq. (18) into Eq. (17), the area function for the spherical parts are given by

$$A_{PS} = \pi h_c(2R - h_c) \quad (20)$$

In this study a series of nanoindentation experimental tests were performed at different indentation loads. However, the spherical part of the area function was neglected based on the very reasonable assumption of all applied loads being performed with $h_c > \delta$.

The deviation in the area function results may be due to indenter tip blunting and this is supported from analysis of the h_d value obtained from the curve best fitting, $h_d = 12.5$.

Troyona and Martin [18] consider the value of h_d to be approximately 6.5 nm for the case of a blunted Berkovich indenter with half induced angle of 70.3° and tip radius of 105 nm. Takeshi [20] determined the distance for four different materials using four different indenters and found it to vary in the range $6.1\text{nm} < h_d < 28.8\text{ nm}$. However tip roundness is not the only factor found to contribute to deviations in values of the area function of an actual indenter. Deformation due to the concentrated residual field stress during indentation will also have effect on the half induced angle, ϕ resulting in change in the value of the constant C. The difference can be noted physically in Eq. (16) between the two values determined from experiment, $C = 30.55$, and theory, $C=24.56$.

5 TIP RADIUS VALUES FROM THE FEM APPROACH

Numerical simulations were performed using commercial ABAQUS finite element code. This code was developed to simulate the Berkovich indentation test. The Berkovich indenter geometry is that of three sided pyramid with total included angle of 142.3 degrees. The Berkovich indenter was modelled as a 2-D asymmetric feature with a spherical cap having a specific tip radius. Figure 8- (a) shows the tip radius modelled with values of projected area function and contact depth obtained from experiment data for a real indenter. As is shown in Fig 8- (b) the specimen was modelled with a linear axisymmetric triangular element type (CAX4R). All specimen sizes used in the simulation were greater than 10 times the maximum indentation depth, which is satisfactorily large, in order to avoid any specimen size effect and boundary effect [21]. The lower surface of the specimens was fixed for all degrees of freedom and one side face was symmetrically fixed in the y-direction. The contact constraint between the indenter and material was defined as the 'master surface (indenter)' and 'slave surface (material)' interaction with a normal contact, to allow the master surface to move and contact the material at all time during the simulation. The contact direction is then obtained in relation to the master surface.

Mesh density under the indenter tip was refined in order to achieve the deformation and stress gradients during indentation to a very high accuracy. The indentation method was simulated in two alternating steps. During the

loading step the indenter was moved in the z-direction in ramp mode and penetrated the specimen until the maximum depth was achieved. The reaction force was recorded at a reference point representing the overall load on the specimen. During the unloading step the indenter was returned to the initial position and same reference point. The loading curve represents the resistance of the material, while the difference between loading and unloading represents the energy loss [22]. Nano-indentation finite element modelling was performed based on the assumption of there being no exponent to the value of strain hardening of the material. Commonly, amorphous materials do not present a predictable strain hardening behaviour [17, 23]. As a consequence, the fused silica was assumed to be an isotropic, linear elastic-perfectly plastic material.

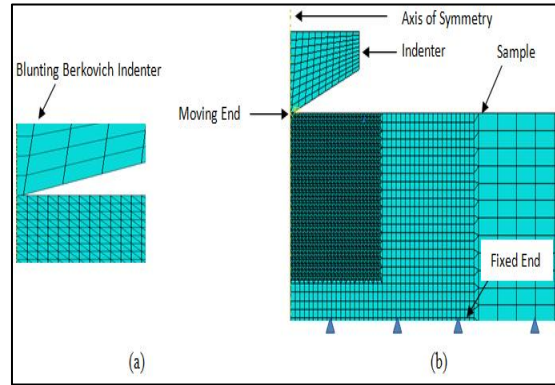


Figure 8 (a) and (b) Finite element boundary condition and mesh density of the indentation process

5.1 Numerical Simulation of Berkovich Indentation Process

The tip radius calculation using best fitting regression analysis of experimental results is very difficult for the Berkovich indenter type due to the size of tip radius (100 nm -200 nm)-which is considered large if compared with the other indenter tip radii. Since the mechanical properties of fused silica are known from the prior instrumented indentation tests, these data were used as input parameters to the FEM simulation. The elastic modulus, estimated from experimental data was $E = 69.91 \text{ GPa}$. This value is very close to the value used by [17] of $E = 70.1 \text{ GPa}$. The yield strength is calculated from a parametric study of the FEM simulations, matching the force displacement curve to the one obtained from a typical experimental result [17]. This analysis delivered a value of $\sigma_y = 6.1 \text{ GPa}$, closely matching the value reported by [17] of $\sigma_y = 5.8 \text{ GPa}$.

The effect of tip radius on the load displacement curves is shown in Figure 9 and is consistent with conventional understanding that a blunted tip will require greater force to penetrate a stated material when compared to a sharp indenter. Furthermore, the loading curve of the elastic-perfectly plastic material is more strongly affected by tip roundness if compared with the unloading curve. Yu [24] reported that the accuracy of mechanical property measurement is principally affected by tip radius blunting especially in nanoindentation. Wang [25] reported that the change in the tip radius results in significant effect on the load displacement data. The authors found the load to increase with a larger tip radius at the same maximum indentation depth.

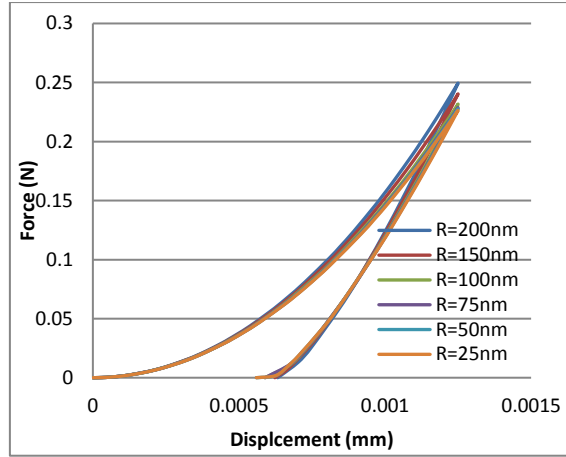


Figure 9 Effect of tip radius on the load displacement curves of fused silica

6 OPTIMIZATION METHOD FOR BERKOVICH INDENTER AREA FUNCTION

A series of FEM simulations were performed for a Berkovich indenter using a wide range of tip radii and indenter inclination angle. Load displacement curves from numerical modelling were compared with experimental results at different indentation load, with best match results obtained employing an objective function. Many optimization methods have been used by researchers to predict the best parameters using single- or multi- objective functions, for example [26, 27]. The main purpose of optimization techniques in our context is to achieve a best fit between the load displacement curve obtained from real measurement results and the curve obtained from numerical analysis. The objective function used in this study is the mean square root error (RMSE). The RMSE value is obtained from determining the difference between experimental and numerical loads for the nano-indentation test Eq. (21)

$$MIN_{OF} = \left[\frac{1}{N} \sum_{i=1}^N (F_{exp-l}^i - F_{num-l}^i)^2 + \frac{1}{N} \sum_{i=1}^N (F_{exp-ul}^i - F_{num-ul}^i)^2 \right]^{1/2} \quad (21)$$

-where F_{exp-l}^i is the measured Force applied in loading at a particular depth, F_{num-l}^i is the value of Force obtained from theory for the loading section of the curve at the same depth predicted by FEM, F_{exp-ul}^i is the measured Force in unloading at a particular depth, F_{num-ul}^i is the value of Force obtained from theory for the unloading section of the curve at the same depth predicted by FEM, and N is the number of sampling points in each test.

Figure 10 shows the comparison between the load displacement curve for numerical theory and experimental results for three different maximum loads. The two curves exhibit good correlation and only a minor deviation occurs in small loads due to the elastic-perfectly plastic material constitutive material law used in the FEM, which is not fully adequate in explaining the behaviour of fused silica material.

Gadelrab [17] reported that the Drucker–Prager model of material densification is more appropriate than the full plastic model in the nanoindentation of fused silica. However, the overall effect of this deviation on the Young's modulus and yield stress is extremely small and thus is ignored in this study. The minimum objective function was determined for the case of tip radius equal to 175 nm, and inclination angle of the Berkovich indenter being within the given tolerance of $69.5^{\circ} \pm 0.15^{\circ}$.

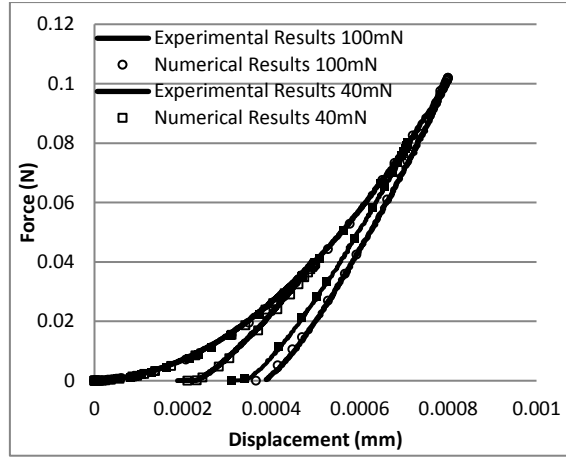


Fig.10 Comparison between numerical and experimental curves using optimal tip geometry

7 AREA FUNCTION VALUES FROM THE FEM APPROACH

Figure 11a shows the 2-D asymmetric FEM employed to calculate the projected area function between the indenter and the specimen. To conduct this method, the nanoindentation load displacement data on the practical reference material with known Young's modulus and Poisson ratio, as well as the corresponding properties of the indenter have to be available. The indenter geometry of tip radius and inclination angle is modelled corresponding to the dimensions obtained using the algorithm developed in previous section.

Figure 11b shows the indenter tip calibration methodology according to guidelines given in Annex B of ISO14577, taking into consideration the Young's modulus and Poisson's ratio of a reference material and $C_f \cong 0$. The projected area and contact depth were calculated using the following series of equations

$$A_p = \pi r_c^2 \quad (22)$$

$$C_t = C_s = \tan\theta \text{ when } C_f \cong 0 \quad (23)$$

$$C_t = \left. \frac{dh}{dp} \right|_{P_{max}} = \frac{\sqrt{\pi}}{2 E_r \sqrt{A_p}} \quad (24)$$

$$h_c = h_{max} - \varepsilon P_{max} C_t \quad (25)$$

A series of FEM simulations were carried out at various indentation loads enabling the indenter projected area A_p to be plotted against contact depth h_c for the examined fused silica reference material. The indenter area function values, determined from the tip geometry and area function algorithm, exhibit only a small dispersion, with the corresponding scatter satisfying ISO14577K-D. Bouzakis [28] reported that nanoindentation FEM supported simulation were carried out using a trial and error methodology, enabling the determination of materials stress-strain constitutive laws and an accurate mathematical explanation of corresponding indenter tip geometry.

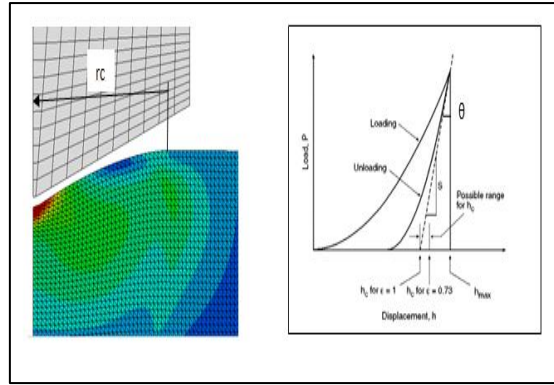


Figure 11 (a) Screenshot of 2-D asymmetric, FEM (b) Indenter tip calibration methodology used to calculate the projected area function

Figure 12 shows the comparison of the indenter projected areas A_P versus the contact depth h_c , according to experimental results and the developed tip geometry FEM algorithm, for the examined reference material. A close correlation is observed between the numerical and experimental data. This informs us that an accurate value of tip geometry and area function can be predicted using the developed FEM based algorithm and reference material. The area function obtained from fitting experimental force displacement curves is found to be larger than the tip metrology from the FEM results. Outcomes of the numerical optimization are also very similar to those obtained with the experimental results, and further, both results yield an area function significantly larger than that for a ‘perfect’ Berkovich indenter, experimental results and the developed tip geometry FEM based algorithm

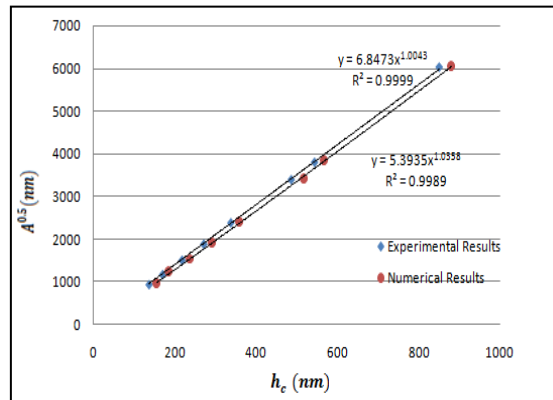


Figure 12 Comparison of the indenter projected areas A_P versus the contact depth h_c

Under all load conditions in this study the elastic modulus determined for fused silica was found to be the same. Based on our findings, indenter calibration using fused silica is deemed a reliable method and overcomes many of the problems encountered with other common materials during indentation testing [29].

8 CONCLUSIONS

Results of nanoindentation measurements for fused silica were analysed and compared with theory. It was found that a linear relationship exists between the total measured compliance, i.e. the inverse of the measured initial unloading slope, $1/S_T$, and the inverse square root of the peak load $(1/P_{max})^{0.5}$. In the case of a known reduced modulus, E_r , the hardness of the test material can be obtained directly from the slope of the fitted $1/S_T$ vs $(1/P_{max})^{0.5}$ straight line. Using the hardness value found from this relationship the projected contact area, A can be determined. Finally, the area function is established by analysing the variation of the projected contact area with the contact depth, h_c .

An important finding in this study is that deviations in the value of the Berkovich indenter area function determined from measurement compared to those for an indenter of perfect geometry may be attributed to the factors: tip blunting and inclination angle deformation, -attributes which are included in the new analysis.

An FEM based algorithm was developed to determine tip geometry and indenter area functions. A parametric study of the simulations allowed a methodology to be developed for calculation of indenter tip geometry and inclination angle, taking into consideration both the Young's modulus and the hardness of reference materials. In this way, the exact contact between the indenter and the specimens can be determined. The calculated indenter area function according to this method is almost identical to the corresponding one expected from ISO14577-4, using fused silica as reference material. A close correlation is observed between the numerical and experimental data for indenter projected areas A_p versus the contact depth h_c .

These outcomes are important for the analysis and characterisation of materials based on both nano- and micro-hardness tests, which is the subject of Part II.

Acknowledgements

This research work was completed with the aid of government and industry support under the 'Innovate UK [TSB] project: Ref. 101275. The authors express their thanks to the industrial partners: Vibraglaz (UK) Ltd, Potters-Ballotini Ltd, Finishing Techniques Ltd, the Manufacturing Technology Centre, Glass Technology Services Ltd and Rolls-Royce plc and to LJMU Research Technician, Mr Peter Moran, for their valued cooperation.

REFERENCES

- [1] Dao, M., Chollacoop, N., Vanvliet, K.J., VenkateshT.A., and Suresh, S. (2001). Computational modelling of the forward and reverse problems in instrumented sharp indentation. *Acta Material*. 49, 2899–2918
- [2] Doerner, M.F., and Nix, W.D. (1986). A method for interpreting the data from depth sensing indentation instruments. *Journal of Material Research*, 1 (4), 601-609
- [3] Oliver, W.C., and Pharr, G.M. (1992). An improved technique for determining hardness and elastic modulus using load and displacement sensing indentation experiment. *Journal of Material Research*, 7 (6), 1564-1583
- [4] Loubet, J.L., Bauer, M. A., Tonck, S. B., and Gauthier-Manuel, B. (1993). Nano-indentation with a surface force apparatus. In *Mechanical Properties and Deformation of Materials Having Ultra-Fine Microstructure NATO ASI Series - Series E. Applied Sciences 233*, 72–89
- [5] Jack, C. H., Bolshakov, A., and Pharr, G. M. (1999). A critical examination of the fundamental relations used in the analysis of nanoindentation data. *Journal of Material Research*, 14 (6), 2296-2305
- [6] Pethica, J.B., Hutchings, R., and Oliver, W.C. (1983). Hardness measurement at penetration depths as small as 20 nm. *Phil. Mag.*, A, 48, 593-598
- [7] McElhaney, K.W., Vlassak, J.J., and Nix W.D. (1998). Determination of indenter tip geometry and indentation contact area for depth-sensing indentation experiments. *Journal of Material Research*, 13, 1300
- [8] Herrmann, K.U., Jennett, N.M., Wegener, W., Meneve, J., Hasche, K., and Seemann, R. (2000). Progress in determination of the area function of indenters used for nanoindentation. *Thin Solid Films*, 377-378, 394-400
- [9] Bolshakov, A., and Pharr, G. M. (1998). Influences of pileup on the measurement of mechanical properties by load and depth sensing indentation techniques. *Journal of materials research*, 13(04), 1049 – 1058
- [10] Cheng, Y.T., and Cheng, C.M. (1998). Relationships between hardness, elastic modulus, and the work of indentation. *Philosophical Mag. Letters*, 78,115 -123

- [11] ISO 14577, Metallic materials Instrumented indentation test for hardness and materials parameters, Part 1: Test method, 2002, Part 2: Verification and calibration of testing machines, 2002, Part 3: Calibration of reference blocks, 2002, Part 4: Test method for metallic and non-metallic coatings, 2007, ISO, Geneva.
- [12] Jianghong, G., Hezhuo, M., and Zhijian, P. (2004). On the contact area for nanoindentation tests with Berkovich indenter: case study on soda-lime glass. *Materials Letters*, 58 1349– 1353
- [13] Martin, M., and Troyon, M. (2003). A critical examination of the P–h² relationship in nanoindentation. *Applied Physics Letters*, 83, 863-865
- [14] King, R.B. (1987) .Elastic analysis of some punches problems from a layered medium. *International Journal of Solids Structure*. 23, N 12, 1657-1664
- [15] Joost, J. V., and Nix, W. D. (1994). Measuring the elastic properties of anisotropic materials by means of indentation experiments. *Journal of the Mechanics and Physics of Solids*, 42 (8), 1223-1245
- [16] Jack, C. Hay, Bolshakov, A., and Pharr, G. M. (1999). A critical examination of the fundamental relations used in the analysis of nanoindentation data. *Journal of Materials Research*, 14 (6), 2296-2305
- [17] Gadelrab, K.R., Bonilla, F.A., and Chiesa, M. (2012). Densification modelling of fused silica under nanoindentation. *Journal of Non-Crystalline Solids*, 358, 392–398
- [18] Martin, M., and Troyon, M. (2002) Fundamental relations used in nanoindentation: Critical examination based on experimental measurements, *Journal of Materials Research*, 17 (9), 2227–2234
- [19] Pharr, M., Oliver, W.C., and Brotzen M. (1992). On the generality of the relationship between contact stiffness. *Journal of Materials Research*, 7, 613-617
- [20] Takeshi, S., and Kohichi, T. (2001). Simplified method for analyzing nanoindentation data and evaluating performance of nanoindentation instruments. *Journal of Materials Research*, 16, (11)
- [21] Knapp, J. A., Follstaedt, D. M., Myers, S. M., Barbour, J. C., and Friedmann, T. A. (2000). Finite element modelling of nanoindentation. *Journal of Applied Physics*, 85, 1460-1471
- [22] Swaddiwudhipong, S., Tho, K. K., Liu, Z. S., and Zeng, K. (2005) Material characterization based on dual indenters. *International journal of solid and structures*., 42, 69-83
- [23] Youn, S.W., Kang, C.G. (2005). FEM study on nano deformation behaviours of amorphous silicon and borosilicate considering tip geometry for pit array fabrication *Material Science and Engineering*, 390, 233-239.
- [24] Yu, N., Polycarpou, A.A., and Conry, T.F. (2004). Tip-radius effect in finite element modelling of sub-50 Nm shallow nanoindentation. *Thin Solid Films*, 450, 295–303
- [25] Wang, T.H., Fang, T.H., Lin, Y.C. (2006). A numerical study of factors affecting the characterization of nanoindentation on silicon. *Material Science and Engineering*, 447 (1–2), 244–253
- [26] Lou J, Lin J, Dean TA. (2006). A study on the determination of mechanical properties of a power law material by its indentation force-depth curve, *Philosophical Mag*, 86, 2881-2905.
- [27] Kang, J.J., Becker, A.A., and Sun, W. (2012). Determining elastic-plastic properties from indentation data obtained from finite element simulations and experimental results. *Int. J. of Mechanical*, 62, (1), 34–46
- [28] Bouzakis, K.-D., and Michailidis, N. (2003). Indenter tip geometries and calibration procedures: deviations in determining coatings “and other materials” mechanical properties. *Material characterization*, 49, 149-156
- [29] David J. Shuman, André L.M. Costa, Margareth S. Andrade. (2007). Calculating the elastic modulus from nanoindentation and microindentation reload curves. *Material characterization*, 58 (4), 380–38